

WaferLLM: A Wafer-Scale LLM Inference System

Congjie He¹, Yeqi Huang¹, Pei Mu¹, Ziming Miao², Jilong Xue², Lingxiao Ma², Fan Yang², and Luo Mai¹

¹University of Edinburgh
²Microsoft Research

Abstract

Emerging AI accelerators increasingly adopt wafer-scale manufacturing technologies, integrating hundreds of thousands of AI cores in a mesh-based architecture with large distributed on-chip memory (tens of GB in total) and ultra-high on-chip memory bandwidth (tens of PB/s). However, current LLM inference systems, optimized for shared memory architectures like GPUs, fail to fully exploit these accelerators.

We introduce WaferLLM, the first wafer-scale LLM inference system. WaferLLM is guided by a novel PLMR device model that captures the unique hardware characteristics of wafer-scale architectures. Leveraging this model, WaferLLM pioneers wafer-scale LLM parallelism, optimizing the utilization of hundreds of thousands of on-chip cores. It also introduces MeshGEMM and MeshGEMV, the first GEMM and GEMV implementations designed to scale effectively on wafer-scale accelerators.

Evaluations show that WaferLLM achieves 200× better wafer-scale accelerator utilization than state-of-the-art systems. On a commodity wafer-scale accelerator, WaferLLM delivers 606× faster and 22× more energy-efficient GEMV compared to an advanced GPU. For LLMs, WaferLLM enables 39× faster decoding with 1.7× better energy efficiency. We anticipate these numbers will grow significantly as wafer-scale AI models, software, and hardware continue to mature.

1 Introduction

Large Language Model (LLM) inference is a rapidly growing workload. It has two phases [14]: (i) the *prefill phase*, which processes input tokens (the prompt) and spends most of its cycles on General Matrix Multiply (GEMM); and (ii) the *decode phase*, which generates tokens one by one in an autoregressive manner, primarily performing General Matrix-Vector Product (GEMV). Decode requires repeatedly loading the entire LLM model into on-chip memory, with GEMV dominating its cycles. Since LLMs generate many tokens, inference is constrained by GEMV latency, making it inherently memory-bandwidth-bound.

To address memory bandwidth bottlenecks, AI accelerators are increasingly adopting system-on-wafer integration [20]. This approach scales chip area to a full wafer, up to 100× larger than a typical GPU die, enabling significantly more on-chip cores, memory and bandwidth. Examples include Cerebras WSE [23] and upcoming Tesla Dojo [38]. The Cerebras WSE-2, for instance, integrates 850,000 cores with 40GB

of on-chip memory—1000× more than GPUs—and provides 22PB/s memory bandwidth, 7000× higher than GPUs. TSMC predicts widespread adoption of system-on-wafer integration due to its performance advantages, energy efficiency in connecting dies, and lowering cost, with IEEE forecasting a wave of wafer-scale computers by 2027 [20].

Unlocking the potential of wafer-scale accelerators is challenging because current LLM systems rely on *shared memory architectures* typical of GPUs and TPUs. Wafer-scale accelerators, however, adopt *network-on-chip* (NoC) designs that interconnect millions of cores with local memory in a *massive-scale, mesh-based memory architecture*. This architecture far exceeds the scale of on-chip crossbars (e.g., one-hop NUMA such as GraphCore IPU), multi-socket NUMA [2], and high-density AI clusters (hundreds of GPUs per pod) [15]. Without fully addressing this fundamental shift in memory architecture, directly applying designs from state-of-the-art systems like T10 [24] and Ladder [41] to wafer-scale devices often results in extremely poor performance.

To address these challenges, we propose a *device model* that captures the critical hardware properties of wafer-scale accelerators, highlighting key differences from shared-memory devices. This model enables us to evaluate current LLM inference design principles, identify non-compliant areas, and pinpoint where new approaches are required. Guided by this model, we can achieve an ambitious system design: *running complete LLM inference on a single chip*, minimizing costly off-chip communication and maximizing on-chip memory bandwidth utilization.

The above idea drives the design of WaferLLM, the first wafer-scale LLM inference system, yielding several contributions:

(1) Device model for wafer-scale accelerators. We propose the PLMR model¹, which captures the following hardware properties of wafer-scale accelerators: (i) **Massive Parallel cores (P)**: Millions of cores can be integrated on a large wafer, requiring systems to effectively partition LLMs and their operations. (ii) **Highly non-uniform memory access Latency (L)**: Inter-core data access exhibits significant variation, with latency differences up to 1000×, necessitating system to mitigate this. (iii) **Constrained local Memory (M)**: Each core has limited memory (tens of KBs to several MBs), requiring efficient memory usage. (iv) **Limited hardware-assisted Routing (R)**: The NoC routing hardware supports small messages

¹PLMR model can be pronounced as “Plummer”

(e.g., a few bytes), with headers and address encoding limited to a few bits, restricting routing paths. Careful communication path planning is crucial to avoid falling back to slower software-based routing.

(2) Wafer-scale LLM parallelism. We propose an effective LLM parallelism method for wafer-scale accelerators, fully compliant with the PLMR model. In the prefill phase, we design fine-grained partitioning to achieve million-core parallelism. For the decode phase, where tensor dimensions are insufficient for partitioning, we design fine-grained replication to enable parallelism with minimal communication costs. As a result, WaferLLM achieves larger-scale and finer-grained parallelism (satisfying P in PLMR) than GPU-based approaches. Additionally, we replace conventional GPU-based GEMM and GEMV operators in existing LLM models with new versions designed for the PLMR model (satisfying L, M and R) and propose tensor placement strategies that eliminate matrix transpositions, costly with a mesh NoC (satisfying L).

We also design a scalable KV-cache management method for wafer-scale devices. This approach features a novel KV cache shift method to ensure balanced core usage (satisfying P and M), avoiding skewed utilization of cores caused by KV cache concatenation methods common on GPUs.

(3) Wafer-scale GEMM. We propose MeshGEMM, a scalable GEMM algorithm for wafer-scale accelerators, enabling WaferLLM to fully accelerate its prefill phase. Unlike conventional distributed GEMM algorithms, MeshGEMM achieves full PLMR compliance by leveraging two key operations: *cyclic shifting* and *interleaving*. Cyclic shifting ensures algorithm correctness while maintaining bounded usage of local memory (satisfying M) and routing resources (satisfying R). The interleaving operation minimizes multi-hop communication in the mesh NoC, effectively reducing the overhead of highly non-uniform memory latency (satisfying L).

(4) Wafer-scale GEMV. We propose MeshGEMV, a scalable GEMV algorithm for wafer-scale devices, enabling WaferLLM to effectively accelerate its decode phase. Unlike existing GEMV implementations, MeshGEMV uses a novel *two-way K-tree allreduce* algorithm to aggregate local GEMV results across massive cores. This algorithm ensures minimal routing resource usage (satisfying R) and reduced communication paths (satisfying L).

We implemented WaferLLM on the Cerebras WSE engine using approximately 7,000 lines of CSL (a C-like programming language) for LLM parallelism, MeshGEMM, and MeshGEMV, and 2,000 lines of Python for loading LLM checkpoints and launching inference.

We conducted end-to-end LLM inference experiments with various models, including full LLaMA3-8B and LLaMA3-13B, as well as subsets of layers of LLaMA3-70B, CodeLLaMA-34B, and QWen2-72B. By combining wafer-scale LLM parallelism, GEMM and GEMV, Wafer-

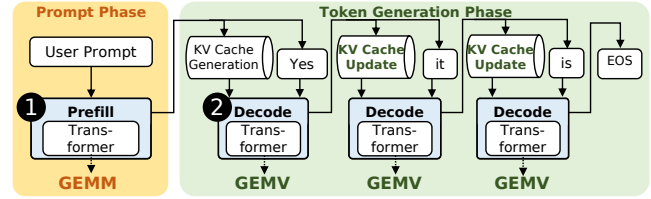


Figure 1: Key components in LLM inference

LLM outperforms state-of-the-art (SOTA) systems: (i) 100-200 \times faster than T10 [24], the SOTA system for massive cores with a distributed on-chip memory architecture, and (ii) 200-400 \times faster than Ladder [41], the SOTA system for shared-memory architectures.

Micro-benchmarks further show that MeshGEMM is 2-3 \times faster than SUMMA [39], the default optimized GEMM for Cerebras WSE, and Cannon [7], the SOTA GEMM for supercomputers with large-scale mesh architectures. MeshGEMV achieves 4-8 \times speedups over Cerebras’s optimized GEMV. Additionally, WaferLLM’s cache shift method is up to 400 \times more scalable than the KV cache SOTA on GPUs, such as PagedAttention [19].

Combining these benefits, WaferLLM (using Cerebras WSE-2) outperforms vLLM (using A100) by 606 \times in GEMV operations and achieves 22 \times better energy efficiency. This comparison is fair, as both WSE-2 and A100 are manufactured using TSMC’s 7nm process. For full LLM inference, WaferLLM delivers a 38 \times faster decode rate (tokens/s) and is 1.7 \times more energy-efficient (token/J) than vLLM. The reduced gains from GEMV to LLM are due to current limitations in Cerebras’s software, hardware, and existing LLM model designs. We anticipate stronger performance as wafer-scale AI computing matures and these limitations are addressed.

2 Background and Motivation

2.1 LLM inference and its key constraint

An LLM inference system typically performs auto-regressive token-by-token generation, as illustrated in Figure 1. The model comprises multiple transformer layers, dominated by self-attention and feedforward blocks. Inference operates in two phases: prefill and decode. The total cycles of the prefill phase are dominated by GEMM operations (shown by ❶). Similarly, the total cycles of the decode phase are dominated by GEMV operations (shown by ❷).

LLM inference is memory bandwidth-bound. Model weights (10-100 GB) must be repeatedly fetched from external memory during inference, as GPUs typically have only 100 MB of on-chip memory. Generating a single token requires transferring tens of GBs, and producing thousands of tokens per second demands hundreds of TB/s bandwidth, far exceeding the capabilities of HBM on current GPUs.

	System-on-Die	System-on-Wafer
Chip Area	400 ~ 800 mm ²	30,000 ~ 160,000 mm ² [38]
# Transistors	10s Billions	Trillions
# Cores	1,000 ~ 10,000s	100,000 ~ 1,000,000s
On-Chip Memory	100s MBs	10s GBs
Memory Bandwidth	TBs/s	10s PBs/s
Attached HBM	10s GBs	TBs (via TSMC SoW)
Die-to-Die Bandwidth	100s GBs/s (via PCB)	10s TB/s (via Wafer)
Die-to-Die Power	10s pJ/bit (via PCB)	0.1s pJ/bit (via Wafer)

Table 1: System-on-Die vs. System-on-Wafer

While tensor parallelism across GPUs can increase bandwidth, mitigating communication bottlenecks in a large GPU cluster remains challenging. Also, adding GPUs improves throughput for concurrent queries but does not reduce response time, as each query is still memory bandwidth-limited.

2.2 Reasons for wafer-scale accelerators

To increase memory bandwidth, accelerator designers are increasingly adopting system-on-wafer integration [20] for several reasons:

Performance advantages. System-on-wafer technology allows trillions of transistors to be integrated into a single wafer-scale chip—100× more than a typical GPU die, shown in Table 1. This enables millions of AI-optimized cores, providing tens of GBs of on-chip memory and up to tens of PB/s memory bandwidth—1,000× higher than a standard GPU’s several TB/s. Future wafer-scale chips can also attach 40–80× more HBM chips to their edge compared to a standard die [20].

Integration efficiency. System-on-wafer excels at integrating massive parallel cores, with wafer-based die-to-die connections offering up to 10× more bandwidth per unit area and nearly 100× better power efficiency per bit than conventional PCB-based I/O (e.g., NVIDIA NVLink), as shown in Table 1.

Lower cost. Wafer-scale integration can lower the manufacturing cost, since the significant fraction of the cost of fabrication (typically 30-50%) is related to testing and packaging the individual chips [44]. Additionally, wafer-scale integration has made notable progress in yield improvement. Companies such as TSMC are also developing techniques to integrate fully tested dies on a single wafer, further enhancing yield.

2.3 Challenges for wafer-scale LLM inference

The key challenge in leveraging wafer-scale accelerators for LLM inference is their shift to a distributed, non-uniform memory architecture on a single chip. Current LLM systems are optimized for shared memory (single chip) or fully connected architectures (e.g., GPU pods), as shown in Figure 2(a). However, as on-chip memory size grows, these architectures face exponential manufacturing costs and performance degradation, driving the need for a distributed on-chip architecture.

AI accelerator designers predominantly use a **mesh-like network-on-chip (NoC)** to connect **massive cores** (ranging

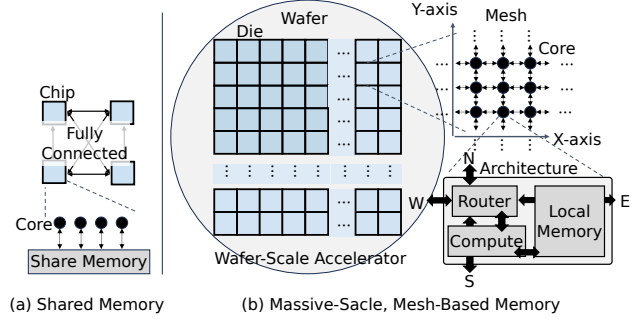


Figure 2: Massive-scale mesh-based memory architecture

from hundreds of thousands to millions), as shown in Figure 2(b). The mesh topology is favored for its efficiency in core arrangement, enabling effective cooling [28], power delivery [18], and cost-efficient wiring [37, 42], with each core communicating only with nearby neighbors, as shown in Figure 2(b). Alternative topologies, such as 3D torus or tree structures, are impractical due to high on-chip wiring costs. Therefore, wafer-scale chip makers such as Cerebras WSE [23] and Tesla Dojo [38] adopt massive-scale mesh architectures. Even non-wafer-scale accelerators such as Meta MTIA [29], Tenstorrent [17], and others [4, 30] use mesh to scale cores on a chip.

The massive-scale mesh architecture presents challenges for several LLM operations due to their high data movement demands: (i) managing LLM models and KV cache, (ii) GEMM operations during the prefill phase, and (iii) GEMV operations during decoding. Other operations, such as element-wise computations such as dot-product and activation functions, require no data movement and naturally benefit from parallelism. Operations needing allreduce, such as RMSNorm and Softmax, can leverage GEMV solutions.

3 Device Model for Wafer-Scale Accelerators

3.1 The PLMR model

We develop the PLMR model to capture the unique hardware properties of wafer-scale accelerators and to motivate system requirements needed for utilizing this emerging hardware.

- (1) **Massive Parallelism (P):** A wafer-scale accelerator can easily be equipped with millions of parallel cores, compared to thousands in GPUs. Each core features a local hardware pipeline that overlaps data ingress, egress, computation, and memory access at the cycle level. This requires the computation to be partitioned at a massive scale and a fine-grained schedule to overlap computation, memory access, and NoC communication.
- (2) **Highly non-uniform memory access Latency (L):** Accessing memory on other cores in a mesh exhibits highly non-uniform latency. In a mesh with $N_w \times N_h$ cores, the maximum NoC hops to a remote core is $\max(N_w, N_h)$. For a million-core mesh, this can reach 1000 hops, causing a

1000 \times latency difference between local and remote memory access. Therefore, it is crucial for the computation to minimize long-range communication whenever possible.

- (3) **Constrained local Memory (M)**: Each core has a small local memory (tens of KBs to several MBs), as performance and energy efficiency decline with larger capacities [43]. As a result, computation data must be explicitly partitioned into fine-grained chunks to fully fit within the constraints of each core’s local memory.
- (4) **Constrained Routing resources (R)**: The message size in the NoC of a wafer-scale accelerator is extremely limited (e.g., a few bytes). This constraint requires message headers (e.g., address encoding) to be restricted to just a few bits, maximizing the capacity for actual data transfer. Consequently, only limited routing paths can be used, and the software system must carefully plan these paths.

We expect these properties to remain relevant, as they are rooted in the fundamental characteristics of hardware and its manufacturing process. The PLMR model applies to both current (Cerebras WSE) and future (Tesla Dojo) wafer-scale devices. Even some non-wafer-scale devices with mesh-based NoC architectures, such as Tenstorrent Blackhole [17], can be represented by PLMR with adjusted parameters for parallelism (P), the size of the mesh (L), or relaxed constraints on local memory (M) and routing resources (R).

3.2 Limitations of state-of-the-art approaches

Leveraging the PLMR model, we analyze why existing AI systems fail to fully utilize wafer-scale accelerators. To run an LLM model on a wafer-scale accelerator, we generally have two choices: (i) abstract the distributed local memory in each core as a shared memory and directly access data placed in a remote core through NoC; and (ii) explicitly partition computation into distributed cores and use message passing to exchange necessary data. We analyze two types of representative systems: LLM runtime or DNN compilers for shared memory architecture such as GPUs, e.g., Ladder [41]; and the SOTA compiler for distributed on-chip memory architectures, e.g., T10 [24] for GraphCore IPU.

Shared-memory system. A shared-memory-based DNN compiler such as Ladder usually assumes a uniform memory access pattern within the underlying memory hierarchy, which cannot tolerate the 1000 \times latency variance in wafer-scale accelerators when accessing data from remote memory (failing in L). Moreover, these compilers [10, 27, 36, 41, 47, 49, 52] often focus primarily on partitioning computation, with less emphasis on optimizing data partitioning. This approach can easily lead to significant data duplication and violate the memory constraint requirements (failing in M). Finally, these compilers are unaware of the communication distance of each core, poorly addressing the constraint of routing resources.

Distributed-memory system. The T10 system [24] is designed for AI accelerators with an on-chip crossbar which

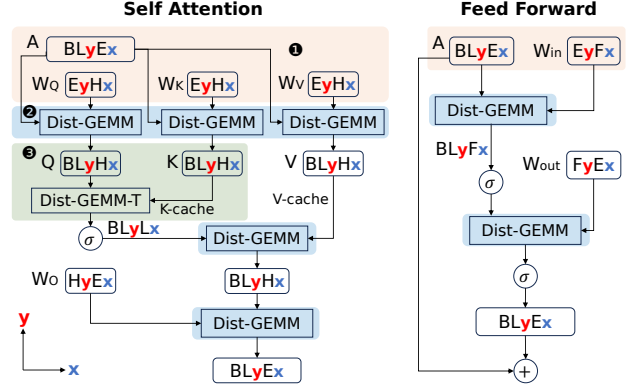


Figure 3: Prefill parallelism plan. $E_x F_y$ represents a matrix of shape $E F$, where the E dimension is partitioned along the x -axis of cores, and F along the y -axis of cores on a mesh.

ensures a constant hop of memory access to other cores on the same chip. T10 handles small local memory and balances communication loads, addressing memory constraints (M) and routing resource limits (R). However, on a PLMR device, it fails to account for varying hop distances (failing in L) and scales to thousands, not millions, of cores (failing in P).

4 Wafer-Scale LLM Parallelism

We present wafer-scale LLM parallelism, featuring new designs across prefill, decode and KV cache management.

4.1 Prefill parallelism

The parallelism for LLM prefill must ensure compliance with the PLMR model. Key challenges include: (i) Handling multiple large matrices during prefill, requiring effective dimension partitioning to achieve million-core parallelism (P); (ii) Optimizing GEMM operations, which involve further partitioning and overlapping computation and communication, to minimize long-range communication overhead (L), respect local memory constraints (M), and account for limited routing resources (R); and (iii) Handling matrix transposes, which are costly on a NoC (L) but often required for sequential GEMM operations.

Designing fine-grained partitioning for million-core parallelism. To achieve high chip utilization, we propose partitioning two dimensions of the input activation and weight matrices along both the X - and Y -axes of cores. This approach enables finer-grained, million-scale parallelism compared to existing methods [12, 14, 31, 34], which typically partition only the embedding dimension, resulting in insufficient parallelism on PLMR devices.

We illustrate this partitioning using self-attention and feed-forward, as shown in Figure 3. For this discussion, we define the following annotations: the input activation A and weight W are multi-dimensional tensors during the prefill process. B represents the batch size, L the sequence dimension, E the

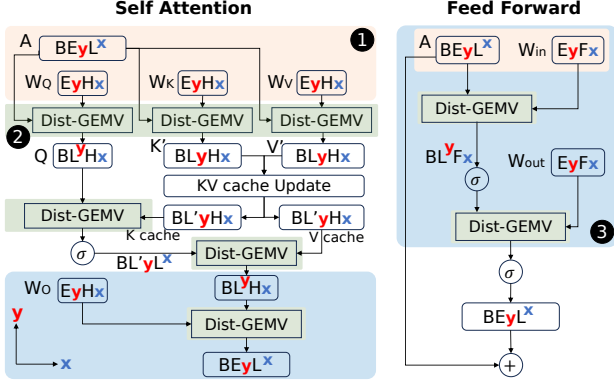


Figure 4: Decode parallelism plan. $E^y F_x$ indicates the E dimension is replicated along the y -axis, and F is partitioned along the x -axis.

embedding dimension, H the head dimension, and F the hidden dimension in the feedforward block. As shown by ❶, the partitioning layout of A is represented as $BL_y E_x$, where the L dimension is partitioned along the Y -axis of cores, and the E dimension along the X -axis of cores. Similarly, all weight matrices (W_Q , W_K , W_V , W_{in} , and W_{out}) are partitioned across both dimensions.

Designing PLMR-compliant distributed GEMM. We propose replacing conventional GEMM operators, designed for shared memory architectures, with a newly designed PLMR-compliant distributed GEMM during the prefill phase (as shown in ❷ of Figure 3). Unlike TPU and GPU systems that primarily rely on allgather operations for GEMM, PLMR-compliant distributed GEMM algorithms achieve high NoC bandwidth utilization while respecting local memory and routing constraints, ensuring compliance with the L , M , and R properties. This PLMR-compliant distributed GEMM is fully described in Section 5.

Using transposed distributed GEMM to avoid matrix transpose. We propose a transpose-free parallelism plan for prefill to avoid matrix transpose, a common operation in LLM systems designed for shared memory architectures. The L property in PLMR highlights that matrix transposition is particularly costly on a wafer-scale device. It requires a core on one corner of the mesh to send data to the opposite diagonal corner, creating a long-range communication path.

Our transpose-free parallelism plan leverages transposed distributed GEMM (denoted as dist-GEMM-T) [11, 39] to compute $Q@K^T$ during LLM prefill, as shown by ❸ in Figure 3. Specifically, the intermediate Q and K tensors, generated by multiplying X with W_Q and W_K , require transposing K before proceeding with dist-GEMM operations due to the on-chip partition shape.

4.2 Decode parallelism

The parallelism strategy for LLM decode must address its memory-bandwidth-intensive nature, presenting several chal-

lenges: (i) Decode uses smaller matrices than prefill due to limited input sequences and batch sizes, requiring careful parallelization when dimensions are insufficient for partitioning; (ii) The phase heavily relies on GEMV operations, which are less compute-intensive than GEMM, resulting in short computation phases with limited overlap with communication, making GEMV vulnerable to long-range communication overhead on a NoC (L) and requiring adherence to local memory and routing constraints (M and R); and (iii) Sequential GEMV operations introduce costly matrix transpose on a NoC, risking violation of the L property.

Designing fine-grained replication to enable parallelism at minimal communication cost. When tensor dimensions are insufficient to achieve the high parallelism required for decode, we propose fine-grained replication of tensors in LLMs, specifically replicating the sequence dimension, where the sequence length equals the prompt length during prefill phase and equals 1 during the decode phase. This approach offers two key advantages: (i) It improves parallelism and ensures balanced loads across all cores, and (ii) It avoids additional communication operations such as allreduce. As shown by ❶ in Figure 4, the E dimension is partitioned along the y -axis, and the L dimension is replicated along the x -axis, represented as $BE_y L_x$. Weight matrices W are partitioned across both dimensions, consistent with the prefill phase.

Our fine-grained replication differs from recent work on long-context/sequence inference systems [45, 50], which selectively replicate certain dimensions during the prefill phase rather than the decode phase.

Designing PLMR-compliant distributed GEMV. We found that existing GEMV implementations fail to fully comply with PLMR requirements due to long-range communication and excessive routing resource consumption at each core. To address this, we propose a PLMR-compliant distributed GEMV, utilizing this new implementation throughout the decode phase (as detailed in ❷ of Figure 4). A comprehensive description of this GEMV design is provided in Section 6.

Pre-optimizing model weight placement to avoid matrix transpose. To avoid matrix transpose during decode, we propose pre-optimizing the model weight layout for decode, particularly for the distributed GEMV operation, to eliminate matrix transpose. While this introduces re-placement overhead between prefill and decode phases, the overhead is far smaller than that of sequential matrix transpose during token generation.

Figure 4 illustrates this proposal, detailed in ❸. Specifically, we optimize the placement of weights such as W_Q and W_{out} for distributed GEMV in decode, differing from their layout in the prefill phase. This approach also removes the need for transpose operations in calculating $Q@K^T$ during decode self-attention.

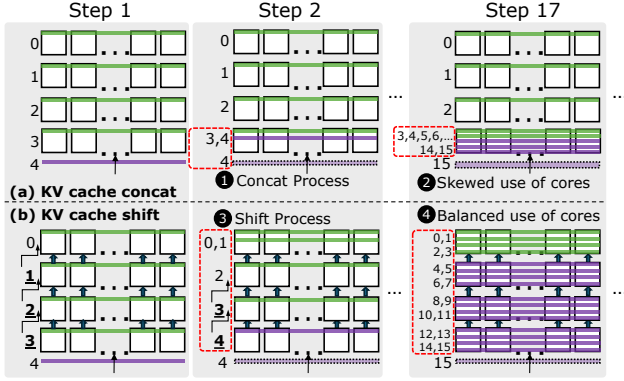


Figure 5: KV cache concatenation vs. KV cache shift

4.3 Shift-based KV cache management

KV cache management on PLMR devices is challenging as it requires storing large data across distributed cores while adhering to local memory constraints (M) and distributing KV cache computations to achieve high parallelism (P). To address these, we have the following insights:

Existing concatenate-based management causes skewed core utilization. Current KV cache management methods primarily concatenate newly generated KV vectors to the existing cache. While efficient in shared memory architectures, this concatenate operation leads to highly skewed core utilization on PLMR devices, as shown in ❶ of Figure 5, where only core in a row is responsible for storing and computing over the newly generated KV vector. After several token generation steps, this only core quickly becomes the bottleneck, as depicted in ❷ of Figure 5, causing skewed memory usage and violating the M in PLMR. Moreover, the imbalanced KV cache distribution across cores results in inefficient parallelism, violating the P property.

Proposing shift-based management for balanced core utilization. We propose a shift-based KV cache management strategy that evenly distributes cache data across all cores. Instead of concatenating new KV cache vectors at the end, this method performs a balancing shift operation, where each row transfers the oldest KV cache data to the row above, as shown in ❸ of Figure 5. When new KV data arrives, each core checks its local capacity against its neighbors. If equal, upward shifts are triggered, with each row receiving data from below and passing some to the row above. As illustrated in ❹, this ensures even KV cache distribution across all cores.

The upward shifts utilize all NoC links in parallel, maintaining high performance and satisfying the P property. The physical placement of KV cache aligns with logical continuity, adhering to the L property. This method also fully resolves the M violation issue observed in the last row of cores with the concatenate-based approach.

4.4 Implementation details

We outline several implementation details below:

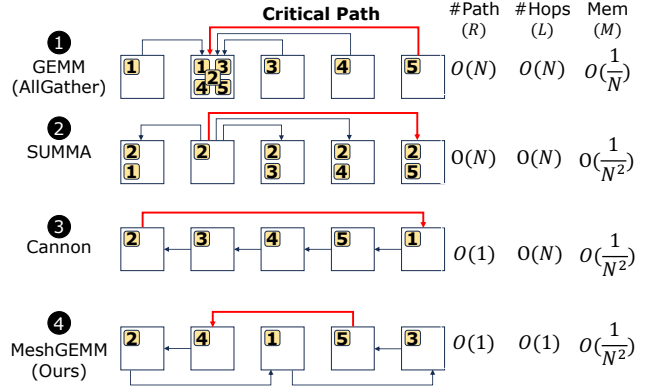


Figure 6: PLMR compliance in distributed GEMM

Prefill and decode transition. Prefill and decode require distinct strategies. To handle the transition efficiently, we reshuffle KV cache and weights through the fast NoC which often provides 100s Pbits/s aggregated bandwidth, completing instantly without relying on slower off-chip memory.

Parallelism configuration. We empirically determine the scalable parallelism for LLM operators. Automatic parallelism configuration is left for future work.

Variations of self-attention. WaferLLM supports variations of Self-Attention, including Grouped Query Attention [3], Multihead Attention [40], and Multi-query Attention [6]. These differ by performing dist-GEMM, dist-GEMV and dist-GEMM-T locally after grouping by head dimensions.

5 Wafer-Scale GEMM

In this section, we introduce MeshGEMM, a scalable distributed GEMM for massive-scale, mesh architectures.

5.1 PLMR compliance in distributed GEMM

To identify an scalable distributed GEMM for PLMR devices, we define the following metrics: (i) *Paths per core*: The number of routing paths per core, with fewer paths ensuring compliance with the R property. (ii) *critical path*: The longest communication path in each step to transmit submatrix (as the red lines in Figure 6), with fewer hops adhering to the L property. (iii) *Memory per core*: The memory required per core, with lower usage ensuring the M property.

We analyze current distributed GEMM methods and show how MeshGEMM meets these metrics:

- (1) **GEMM via Allgather** is commonly used in GPU and TPU pods for distributed GEMM [31, 34, 51]. Its longest communication path in each step is one core gathering data from the farthest cores, shown as the red line in Figure 6 ❶, and N steps to complete the allgather. Each core creates N communication paths to neighbors in its row and column (violating R). The gather in each step spans the critical path with $O(N)$ hops (violating L), and

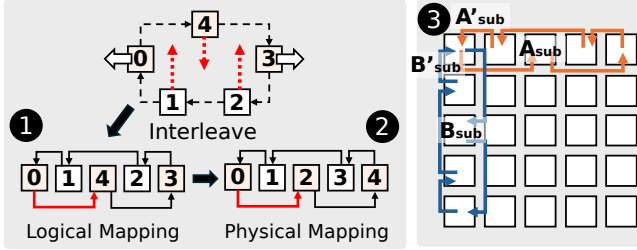


Figure 7: Design intuitions and scalability analysis.

each core uses $O(1/N)$ memory due to inflated working buffers, far exceeding the $O(1/N^2)$ for local submatrices (violating M).

- (2) **SUMMA** is Cerebras’ default choice for distributed GEMM on its wafer-scale engine [8]. Its longest communication path in each step is where one core broadcasts data to the farthest core along the column or row, shown by the red line in ② of Figure 6. Every core creates N communication paths (violating R) and spans the critical path with $O(N)$ hops (violating L) in the longest path. While SUMMA improves memory usage compared to AllGather, requiring only a working set equal to the size of locally partitioned submatrices, it still doubles memory usage.
- (3) **Cannon** is mesh-optimized choice for distributed GEMM [7], popular in supercomputers. Its longest communication path in each step is the head cores send data to the tail cores. As shown in ③ of Figure 6, each core communicates with two neighbours in a 2D torus, and only needs $O(1)$ communication paths and optimal memory usage of $O(1/N^2)$. However, it incurs the critical path with $O(N)$ hops as the red line, violating L.
- (4) **MeshGEMM (Ours)** is a distributed GEMM which complies with the PLMR model. Its longest communication path in each step is shown as the red line in ④ of Figure 6. Each core communicates with two neighbors, two hops away (proven in later sections to be scalable for mesh architectures). This design achieves $O(1)$ communication paths per core needed and optimal memory usage of $O(1/N^2)$, similar to Cannon. Crucially, it bounds the critical path to 2 hops with $O(1)$ complexity, making it uniquely capable of addressing the L property.

5.2 Design intuitions and scalability analysis

Our design involves two steps: (i) We ensure algorithm correctness using a cyclic shifting process for GEMM, and (ii) We prove that two-hop communication on this cycle is the minimal distance required to satisfy the L property.

Cyclic shifting. Cyclic shifting enables MeshGEMM to satisfy the M and R properties by limiting communication to two neighbors and minimizing memory usage. It ensures correct GEMM results, following reasoning similar to Cannon [7].

Algorithm 1: INTERLEAVE

Input: index, N
Output: send_index, recv_index

```

1 if index mod 2 == 0 then
2   |   recv_index = Max (index - 2, 0);
3   |   send_index = Min (index + 2, N - 1);
4 else
5   |   recv_index = Min (index + 2, N - 1);
6   |   send_index = Max (index - 2, 0);
7 if index == 0 then recv_index = 1;
8 if index == N - 1 then
9   |   if N mod 2 == 0 then recv_index = N - 2;
10  |   else send_index = N - 2;
11 Return send_index, recv_index;
```

As illustrated in ④ of Figure 6, a logical circle of 5 cores is flattened into the physical communication mapping, with a critical path from head core to tail core.

Interleaving. For the flatten communication plan, we would like to minimize the length of the critical path further, thus satisfying the L property. Our key intuition here is to introduce an INTERLEAVE operation to find the mapping relationship from logical to physical, defined in Algorithm 1. As shown by ① of Figure 7, MeshGEMM first insert core 1 in between core 0 and 4 and core 2 in between core 4 and 3 to form a logical mapping, and then call the INTERLEAVE operation to get the send to and receive from neighbours’ index, resulting in a permuted, equivalent communication plan as shown by ② in Figure 7. For example, there are 5 cores total ($N=5$), so physical core 2 (index=2) sends data to physical core 4 (send_index=4) and receives from physical core 0 (recv_index=0).

Scalability analysis. We can prove that the two-hop distance created by INTERLEAVE cannot be further reduced. The proof relies on the fundamental properties of sequential arrangements: if we attempt to create a circular sequence where each number differs from its neighbors by exactly one hop, we encounter a mathematical impossibility. This can be understood by visualizing the numbers as points on a line - while adjacent numbers can be connected, the endpoints of the sequence cannot simultaneously maintain single-hop differences with their neighbors while forming a circle.

Note that our discussion, based on a 1D array, naturally extends to a 2D mesh, as the 1D array corresponds to the mesh’s X-axis and Y-axis due to their symmetry.

5.3 The MeshGEMM algorithm

We outline the key steps of MeshGEMM below:

- (1) **Initialization:** Consider $C = A \times B$. MeshGEMM will partition A and B into tiles A_{sub} and B_{sub} along two dimensions, forming $N \times N$ tiles, which are distributed across

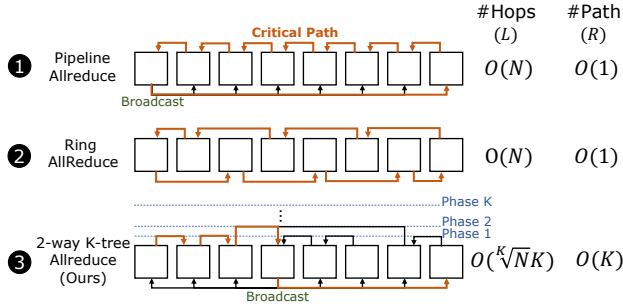


Figure 8: PLMR compliance in distributed GEMV

the cores. Each core receives one tile of A_{sub} and one of B_{sub} . MeshGEMM will then use INTERLEAVE to initialize the neighbor’s positions for each core.

- (2) **Alignment:** Each core will then align with neighbors to align the input submatrices in a way that ensures every core in the distributed system begins with the appropriate operands for the matrix multiplication process.
- (3) **Compute-shift loop:** Each core operates with a compute-shift loop involving N steps of communication and computation. In each step, every core computes the partial sum of its corresponding $C_{sub} = A_{sub} \times B_{sub} + C_{sub}$. Meanwhile, shift A_{sub} along the X-axis and B_{sub} along the Y-axis to get new A'_{sub} and B'_{sub} for the next step computation as ③ we shown in Figure 7. After N steps, the accumulated C_{sub} is returned.

5.4 Implementation details

Handling non-square mesh. For a non-square mesh $N_h \times N_w$ ($N_h \neq N_w$), the A and B matrices can be logically partitioned into $N_{lcm} \times N_{lcm}$ cores, where N_{lcm} is the least common multiple of N_h and N_w .

Transposed distributed GEMM. The above algorithm key steps can be applied to the computation of $C = A \times B^T$, the dist-GEMM-T in Figure 3 to avoid transposing B on mesh. It does not require alignment before computation and only necessitates N steps two-hop compute-shift for the right matrix B along the Y-axis. After each shift step, each core computes $C_{sub} = A_{sub} \times B_{sub}$, followed by a ReduceAdd of C_{sub} along the X-axis. After N steps, the final matrix C is obtained.

6 Wafer-Scale GEMV

In this section, we describe MeshGEMV, a scalable GEMV algorithm for PLMR devices.

6.1 PLMR compliance in distributed GEMV

The completion time of a distributed GEMV is primarily determined by an allreduce operation that aggregates partial results from all selected cores and broadcasts the aggregated

results back to all cores. So, we define the number of add-operations (hops) in the longest aggregation path as the *critical path* in GEMV. Below, we analyze common distributed GEMV implementations in LLM systems and demonstrate that MeshGEMV is the only approach fully compliant with the PLMR model.

- (1) **GEMV with pipeline allreduce** is commonly used in TPU pod systems [34] and as the default in Cerebras demo [9]. As shown by ① in Figure 8, it bounds routing resource usage to $O(1)$ per core (meeting R in PLMR). However, its longest aggregation path is from tail to head cores, as shown in the red line, and spans the critical path at $O(N)$, violating the L property.
- (2) **GEMV with ring allreduce** is commonly used in GPU pod systems, where it is the default configuration. As shown by ② in Figure 8, it bounds routing resource usage to $O(1)$ (meeting R in PLMR). However, it spans $O(N)$ hops in the critical path, violating the L property.
- (3) **GEMV with two-way K-tree allreduce (Ours).** As shown by ③ in Figure 8, we build a balanced K-tree to reduce from two-way; its longest aggregation path is from the head or tail core to the tree root core. The critical path is $O(\sqrt[K]{NK})$ which can address the L. The max number of communication paths at each root core is $O(K)$, and can meet the R limitation by adjusting the K.

6.2 The MeshGEMV algorithm

We will outline the key steps of MeshGEMM below:

- (1) **Initialization:** Consider $C = A \times B$ and A is a vector. MeshGEMV will partition B into tiles B_{sub} along two dimensions, forming $N \times N$ tiles and distributed across the cores. For A , MeshGEMV will partition it along the vector length, forming N tiles distributed on one axis and replica A on another axis. Each core receives one tile of A_{sub} and one of B_{sub} . Then we determine which cores form a group to obtain aggregated results in each phase based on the K-tree.
- (2) **Parallel computation:** In this stage, each core performs a local GEMV $A_{sub} \times B_{sub}$ to obtain C_{sub} partial sum.
- (3) **Aggregation:** The aggregation step primarily involves using the two-way K-tree allreduce we design. The key steps as follows: (i) In the 1st-phase, each group performs group reduction and obtains the partial sum of C_{sub} at the root core of each group. (ii) In the k th-phase, the results from the $(k - 1)$ th-phase are reduced to the root cores of each group in the k th-phase. After K times repeating, C can be obtained by concatenating the C_{sub} from all K-tree root cores. (iii) Optionally, a broadcast operation from the root core of the K-tree may follow, depending on whether continuous GEMV is required.

Scalability Analysis. As shown in ① of Figure 8, this method scales efficiently with parallelism and meets the L property

by selecting an appropriate K . It requires $K + 1$ paths at the tree root core but allows flexible adjustment of K to address R based on hardware limitations.

However, a larger K is not always better, as it depends on N and R constraints. Additionally, larger K increases routing complexity and overhead. Considering these factors, we have chosen $K = 2$ for our current implementation evaluated in the following sections.

7 Evaluation

We extensively evaluated WaferLLM against various state-of-the-art methods and systems. Our results show that:

- (1) WaferLLM achieves orders of magnitude speedup over T10 and Ladder in LLM inference (§7.1);
- (2) WaferLLM’s MeshGEMM and MeshGEMV achieve strong performance and scalability over state-of-the-arts (§7.2);
- (3) WaferLLM’s shift-based KV cache management enables over $360\times$ more token capacity (§7.4);
- (4) WaferLLM on Cerebras WSE-2 achieves up to $38.6\times$ throughput and $1.7\times$ energy efficiency compared to vLLM on A100 in LLM inference (§7.5).

Experiment setup. We evaluate WaferLLM on a server with Cerebras WSE-2. WSE-2 has 850,000 Cores, each with a Compute Engine (CE) operating at a maximum 1.1 GHz. Each clock cycle can fetch two 32-bit operands from SRAM, perform a multiply-accumulate operation, and then write back to SRAM. Each core also has a fabric router that can send or receive 32-bit messages from neighbouring cores with a single clock cycle. Additionally, each core contains 48KB of SRAM, with the chip totalling 40GB of aggregated SRAM [23].

We compare WaferLLM with two DNN compilers: (i)T10 [24], the state-of-the-art compiler for AI accelerators with inter-core connections and distributed on-chip memory, and (ii)Ladder [41], the state-of-the-art compiler for shared memory architectures. For T10, we implemented it on WSE-2, treating each core as part of a distributed memory system interconnected by a crossbar, despite the actual mesh topology. T10 maps data to core IDs and fetches data from local SRAM as required. For Ladder, we treated the distributed memory architecture of the chip, interconnected by mesh, as unified memory, requiring collective communication over the NoC to access data.

LLM models. Our evaluation includes various representative LLMs of different sizes and architectures. Specifically, LLaMA3-8B and LLaMA2-13B are widely used open-source LLMs, with LLaMA3 using group-query attention instead of multi-head attention to reduce KV cache usage. CodeLLaMA-34B is a specialized LLM for coding tasks, while QWen2-72B, another popular LLM, is renowned for its high model quality.

Model	SeqLen In/Out	2048/128	4096/128	2048/2048	4096/4096
LLaMA3-8B	WaferLLM	764.4	604.38	2370.33	2480.4
	T10	4.6	4.5	58.3	94.6
	Ladder	1.18	1.05	7.4	8.72
LLaMA2-13B	WaferLLM	473.9	413.98	1690.28	1848
	T10	2.6	2.51	35	58.27
	Ladder	0.7	0.69	4.93	6.14

Table 2: End-to-end LLM inference throughput (tokens/s)

7.1 LLM inference

We first report the end-to-end performance of WaferLLM compared to T10 and Ladder. To provide deeper insights, we further analyze the performance by breaking down the execution into prefill and decode phases.

End-to-end throughput. Table 2 shows the inference throughput (i.e., tokens per second) of LLaMA3-8B and LLaMA2-13B on different configurations of input and output sequence length. WaferLLM uses core configurations optimized for the best performance with each model. In LLaMA3-8B, we use 660×660 cores for prefill and 360×360 for decode. In LLaMA2-13B, we use 750×750 cores for prefill and 375×375 for decode. CodeLLaMA-34B and QWen-72B are not included due to the memory constraint of WSE-2.

Compared to T10, WaferLLM achieves $160\times$ speedup on average, up to $180\times$, for short sequence generation tasks such as 4096 and 2048 input context lengths with 128 tokens output. For longer tasks, with input context lengths of 4096 and 2048 tokens and output lengths of 4096 and 2048 tokens, WaferLLM achieves $36\times$ on average and up to $48\times$. Although T10 designs the compute-shift model that considers the memory constraints (M) and routing resource limits (R) of a PLMR device, it does not account for the cores interconnected by a mesh NoC. thus failing to address varying hop distances (L) and scale to millions of cores (P), highlighting the need for new system designs in massive-scale NUMA architectures.

Compared to Ladder, WaferLLM achieves $625\times$ speedup on average, up $677\times$, for short sequence generation tasks such as 4096 and 2048 input context lengths with 128 tokens output. For longer sequence generation tasks, with input context lengths of 4096 and 2048 tokens and output lengths of 4096 and 2048 tokens, WaferLLM achieves $312\times$ on average and up to $342\times$. That is because Ladder is designed for shared memory architecture and does not consider the characteristics of the PLMR device, resulting in failure in partitioning LLMs across millions of cores (P), incurring costly long-range NoC communication (L), failure in handling local memory constraints (M) and limited routing resources (R).

Prefill throughput. Table 3 shows the prefill throughput (i.e., input tokens processed per second) for an input sequence length of 4096, using core configurations from 480×480 to 720×720 . For CodeLLaMA-34B and QWen2-72B, which exceed the memory capacity of WSE-2, we evaluate a subset of layers and scale the results proportionally due to their

Model	Core Config	480×480	600×600	720×720
LLaMA3-8B	WaferLLM	20320.6	25037.22	27686.45
	T10	175.01	156.62	132.82
	Ladder	61.82	42.31	31.32
LLaMA2-13B	WaferLLM	13685.10	16854.21	17498.28
	T10	121.02	100.53	81.28
	Ladder	47.25	33.14	24.23
CodeLLaMA-34B	WaferLLM	5471.43	7540.13	8526
	T10	49.06	46.77	41.23
	Ladder	30.01	23.14	17.67
QWen2-72B	WaferLLM	2785.19	3775.53	4421.58
	T10	24.89	23.48	21.50
	Ladder	16.77	12.80	10.12

Table 3: Prefill throughput (tokens/s)

Model	Core Config	420×420	540×540	660×660
LLaMA3-8B	WaferLLM	2699.94	2501.54	2243.25
	T10	418.27	339.43	265.12
	Ladder	14.6	13.09	11.42
LLaMA2-13B	WaferLLM	2039.22	1899.4	1739.78
	T10	341.83	270.79	233.72
	Ladder	11.01	9.93	9.07
CodeLLaMA-34B	WaferLLM	1450.77	1407.68	1359.18
	T10	278.24	222.41	222.41
	Ladder	6.07	6.15	5.77
QWen2-72B	WaferLLM	839.71	824.3	787.08
	T10	168.5	132.97	114.56
	Ladder	3.23	3.29	3.38

Table 4: Decode throughput (tokens/s)

uniform layer structure.

WaferLLM achieves significant speedups over T10 and Ladder by effectively addressing all PLMR properties. As discussed in §2, GEMM is the primary bottleneck, and MeshGEMM substantially enhances WaferLLM’s prefill performance, analyzed in detail in §7.2.

Additionally, WaferLLM scales throughput with increasing cores across all models. For instance, WaferLLM achieves a 1.6× scaleup on QWen2-72B and a 1.4× scaleup on LLaMA3-8B when scaling from 480×480 to 720×720 cores. This improved scalability is primarily because larger models better utilize the device’s compute resources, reducing the relative impact of NoC communication. In contrast, T10 and Ladder fail to scale effectively, with throughput even declining as more cores are added, due to persistent communication latency bottlenecks.

Decode throughput. Table 4 shows decode throughput for core configurations from 420×420 to 660×660. For CodeLLaMA-34B and QWen2-72B, we evaluate a subset of layers and scale the results.

By addressing all PLMR properties, WaferLLM achieves an average speedup of 5.7× (up to 6.5×) over T10 and 217× (up to 260×) over Ladder with 420×420 cores.

Unlike prefill, decode throughput may decrease with more cores due to increased NoC communication latency, which impacts GEMV performance. Additionally, decode’s 6.5X improvement over T10 is less than prefill’s 160X because it involves less data transfer, limiting WaferLLM’s communication advantage.

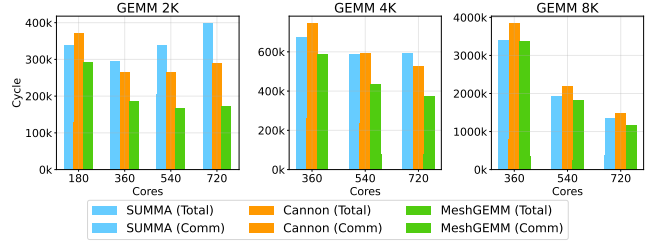


Figure 9: MeshGEMM vs. SUMMA vs. Cannon

7.2 MeshGEMM

We compare MeshGEMM with Cannon [7] and SUMMA [39] across different core scales and matrix sizes.

Scaling the number of cores. Figure 9 shows MeshGEMM with a fixed matrix size while scaling the number of cores. MeshGEMM achieves the lowest execution cycles by leveraging the INTERLEAVE operation to minimize communication overhead. It demonstrates stronger scalability, maintaining over 70% computational efficiency even near the hardware limit. In contrast, SUMMA and Cannon exhibit poor scalability, with computational efficiency falling below 50% with 720×720 cores, primarily due to high communication overhead.

Additionally, increasing the cores does not consistently yield benefits. In GEMM 2K, scaling cores from 540×540 to 720×720 demonstrates diminishing returns: while computational cycles decrease, the additional communication overhead from more rounds of shifting negates these benefits. As a result, the total execution cycles for Cannon and SUMMA worsen significantly. In contrast, MeshGEMM mitigates these effects effectively, allowing further core scaling if required to address other constraints, such as the need for larger aggregate memory to accommodate data.

An interesting observation in Figure 9 is that for GEMM 8K, communication cycles decrease as core count increases. This occurs because GEMM 8K processes large data volumes and has lengthy computations, allowing full overlap with communication. In this scenario, communication becomes bandwidth-bound rather than latency-bound, and increasing core count boosts aggregated network bandwidth, resolving the bottleneck.

Scaling matrix size. We also evaluate MeshGEMM with larger matrix sizes, transforming GEMM into a more compute-intensive operation. At large scales, though the cost of communication becomes less significant, MeshGEMM maintains its scalability and outperforms SUMMA and Cannon by a wide margin, reducing total cycles by around 17%.

7.3 MeshGEMV

We evaluate MeshGEMV and the default GEMV implementation on Cerebras (pipeline allreduce) across various core scales and matrix shapes.

Scaling the number of cores. Figure 10 shows MeshGEMV

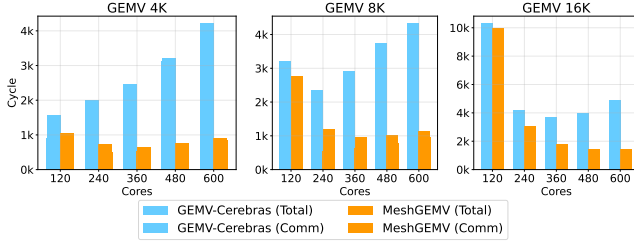


Figure 10: MeshGEMV vs. GEMV-Cerebras

Model	LLaMA3-8B	LLaMA2-13B
Concat-based (PagedAttention)	382	16
Shift-based (WaferLLM)	137548	6168

Table 5: Maximum tokens in generation

with a fixed matrix size across an increasing number of cores. Compared to the baseline method, MeshGEMV significantly reduces communication cycles due to the efficient Two-way K-tree AllReduce, saving communication time and improving overall execution time by up to $4.6\times$.

As the number of cores increases, the communication cost for MeshGEMV increases only slightly. In contrast, the baseline method’s linear reduce steps become increasingly costly as the number of cores increases, resulting in substantial performance degradation with more cores.

Scaling matrix size. We also evaluate MeshGEMV with larger matrix sizes. At larger scales such as 16K, MeshGEMV maintains great scalability, with total execution cycles continuing to decrease as more cores are added. This contrasts with the baseline method, where a clear transition is observed: the savings in computational cycles diminish with increasing cores, and eventually result in negative gains.

7.4 Shift-based KV cache management

We also compare the shift-based KV cache management with the concat-based KV cache management implemented in PagedAttention. We evaluate KV cache capacity on LLaMA3-8B and LLaMA2-13B using the same settings as the end-to-end inference evaluation in §7.1. Table 5 shows that WaferLLM’s shift-based KV cache management supports $360\times$ and $385\times$ more tokens than the concat-based method for LLaMA3-8B and LLaMA2-13B, respectively. This improvement results from balanced core utilization and the resolution of skewed data issues achieved by the shift-based approach.

7.5 Comparison with GPUs

Finally, we compare WaferLLM against the SOTA LLM inference system on GPUs. For this experiment, we use Cerebras WSE-2 and NVIDIA A100, both manufactured on TSMC’s 7nm process, ensuring a fair comparison. To compare against the H100 fairly, we would need access to the WSE-3 which is unavailable for us.

GEMV	[1,16K]×[16K,16K]	[1,32K]×[32K,32K]
MeshGEMV(WSE-2) Time (ms)	0.0012	0.00203
cuBLAS(A100) Time (ms)	0.336	1.231
WSE-2/A100 Energy Ratio	10.37	22.46

Table 6: Comparing MeshGEMV(WSE-2) with cuBLAS(A100) in GEMV latency and energy.

GEMM	[16K,16K]×[16K,16K]	[32K,32K]×[32K,32K]
MeshGEMM(WSE-2) Time (ms)	4.8	34
cuBLAS(A100) Time (ms)	34.4	282.1
WSE-2/A100 Energy Ratio	0.265	0.307

Table 7: Comparing MeshGEMM(WSE-2) with cuBLAS(A100) in GEMM latency and energy.

GEMV. We compare MeshGEMV with GEMV on GPUs, isolating the difference in numerical operators that Cerebras has yet to optimize fully compared to CUDA. Shown by Table 6, for a cuBLAS implementation GEMV [32], MeshGEMV outperforms GPU by $606\times$ in completion time, showcasing the advantages of providing substantial memory bandwidth through wafer-scale devices. This translates to $22\times$ greater energy efficiency, reflecting the benefits of wafer-based connections (connecting on-chip memory) over PCB-based ones (connecting off-chip HBM) in GPUs.

Despite these advantages, MeshGEMV does not achieve the theoretical $7,000\times$ improvement. Profiling identifies three contributing factors: (i) WSE-2 cores, still in their second generation, cannot fully overlap memory access and computation; (ii) edge cores are underutilized; and (iii) NoC long-range communication overhead persists, despite MeshGEMV mitigating it effectively. We anticipate these gaps will continue to narrow as wafer-scale accelerators mature.

GEMM. Cerebras WSE-2 offer limited benefits for GEMM, since energy-efficient wafer-based connections do not address its compute bottleneck. Performance ultimately hinges on the density of transistors and the efficiency of the core design, which is reflected by the specification of Cerebras WSE-2 (i.e., 50% less energy efficient than A100 GPU).

In absolute performance, MeshGEMM is $8.3\times$ faster than CUDA GEMM, as shown in Table 7, largely due to its larger on-chip area. However, this speedup does not translate into energy savings. MeshGEMM is observed to be 70% less energy efficient than GPU GEMM, a gap expected to narrow with improved core designs, as seen in Cerebras WSE-3, which increases core efficiency by 100% .

LLM inference. Finally, we compare WaferLLM with vLLM for running LLM inference, shown as Table 8. Unlike isolated GEMV and GEMM comparisons, full LLM inference include numerous system components that WaferLLM does not optimize and are limited by the current maturity of the Cerebras software stack (e.g., less optimized numerical operators compared to NVIDIA CUDA). Despite these constraints, WaferLLM achieves 2480 tokens/s and 1848 tokens/s throughput for LLaMA3-8B and LLaMA2-13B, respectively, translating

Sequence Input 4096 / Output 4096	LLaMA3-8B	LLaMA2-13B
WaferLLM(WSE-2) Throughput (tokens/s)	2480.4	1848
vLLM(A100) Throughput (tokens/s)	78.36	47.86
WSE-2/A100 Energy Ratio	1.41	1.71

Table 8: Comparing WaferLLM(WSE-2) with vLLM(A100) in end-to-end throughput and energy.

to $31.6\times$ and $38.6\times$ speedup and approximately $1.4\times$ and $1.7\times$ better energy efficiency in tokens per joule.

The reduction in energy efficiency from GEMV’s $22\times$ to LLM’s $1.7\times$ stems from two factors: (i) WSE-2 cores have limited local SRAM (48KB), preventing efficient tensor parallelism as in vLLM and necessitating pipeline parallelism, which introduces execution bubbles and reduces chip utilization by $5\times$; and (ii) LLaMA models are optimized for GPU architectures, with narrow layers designed to minimize off-chip overhead. This limits layer placement across WSE-2 cores, exacerbating bubble issues.

8 Current Limitations and Future Directions

We discuss the current limitations of WaferLLM and wafer-scale accelerators and envision their future solutions:

Hardware architecture. The performance of WaferLLM is currently constrained by execution bubbles caused by the need for pipeline parallelism. Increasing a core’s compute efficiency and local memory by $5\text{-}6\times$ could mitigate the need for pipeline parallelism, enabling more efficient tensor parallelism, as on vLLM. This adjustment could boost LLM decode speed, potentially reaching 10,000 tokens per second for Llama-13B on a single chip.

LLM model design. The limited bandwidth of HBM has constrained today’s LLM model designs from using large tensors in transformer layers [5, 16]. With the advent of wafer-scale accelerators, we anticipate new LLM architectures adopting larger tensors (for example, the architectures with significantly wider layers than those today), free from hardware limitations, and avoiding the bubble issues when supporting current LLMs in WaferLLM.

Beyond Cerebras WSE. Although evaluated with Cerebras WSE, the PLMR model applies to future devices such as Tesla Dojo, featuring hundreds of thousands of cores connected via a mesh, each with MBs of local memory and limited NoC routing. Future devices may adopt different mesh-like architectures with shorter NoC paths, such as 2D torus or hybrids with on-chip switches, all consistent with the PLMR model. Our wafer-scale LLM parallelism will continue to support these architectures effectively. MeshGEMM and MeshGEMV address the worst-case 2D mesh scenario and will remain better, at least not worse, than baseline methods.

TSMC’s newer System-on-Wafer integration, expected in 2027, could boost chip density by $40\times$ on a wafer while still aligning with the PLMR model, ensuring the long-term relevance of our contributions.

9 Related Work

Deep learning frameworks and compilers. Current deep learning frameworks and compilers, such as PyTorch, TensorFlow, and XLA [1, 10, 27, 33, 35, 36, 41, 47, 49, 52], are designed for shared memory architectures and use a tile-based “load-compute-store” computation model. While effective for shared memory, this model ignores the unique characteristics of PLMR devices, making it inefficient for wafer-scale AI chips. LLM frameworks such as vLLM and TensorRT-LLM [19, 51] have emerged to support modern LLMs but rely on frameworks and compilers designed for shared memory architectures (e.g., PyTorch [33]), inheriting similar limitations on wafer-scale chips.

Distributed GPU and TPU systems. The on-chip distributed memory architecture could theoretically be treated as a distributed LLM system, as studied in prior works [19, 22, 34, 45, 48, 51]. However, such systems, designed for GPU and TPU pods (up to thousands of nodes), rely on more capable routers and lack local memory constraints, making them misaligned with the PLMR model. These approaches are complementary to our focus on on-chip scaling.

Systolic array. Systolic array architectures [21], used in AI accelerators such as Amazon Trainium and Google TPU, focus on the design of small cores rather than larger wafer-scale accelerators. With limited processing elements (usually up to hundreds) in a core, they are not PLMR devices but complement WaferLLM. For example, a Cerebras WSE core could employ a systolic array to accelerate local GEMM operations.

Dataflow architectures. Prior research has explored computation on dataflow architectures that account for inter-core connections. TENET [25] maps computation spatially and temporally to connected cores in a dataflow pattern. DISTAL [46] enables scheduling over distributed clusters using a dataflow approach. SambaNova [13] combines model and pipeline parallelism for DNN execution. However, none of these works scale computation to wafer-scale chips.

Wafer-scale allreduce. Recent research [26] has investigated wafer-scale allreduce, but a single allreduce cannot fully parallelize GEMV or support full LLM inference as achieved by WaferLLM. Additionally, this prior work is a specific instance of the two-way K-tree allreduce proposed in WaferLLM.

10 Conclusion

We envision this paper as a foundational step in exploring the potential of wafer-scale computing for LLMs. The simple yet effective PLMR model has revealed significant opportunities, guiding the development of the first wafer-scale LLM parallelism solution and scalable GEMM and GEMV algorithms for wafer-scale accelerators. Despite the limitations of the current software stack for wafer-scale devices, our approach achieves orders-of-magnitude improvements in both

performance and energy efficiency. We hope this work inspires greater focus on wafer-scale computing and advances the path toward a more sustainable future for AI.

References

- [1] M. Abadi, P. Barham, J. Chen, et al. TensorFlow: A system for large-scale machine learning. *OSDI 2016*, 2016.
- [2] Advanced Micro Devices. AMD optimizes EPYC memory with NUMA. White paper, Advanced Micro Devices, Inc., 2023.
- [3] Joshua Ainslie, James Lee-Thorp, Michiel de Jong, Yury Zemlyanskiy, Federico Lebrón, and Sumit Sanghai. Gqa: Training generalized multi-query transformer models from multi-head checkpoints, 2023.
- [4] AMD. AMD XDNA adaptive architecture, 2023. Accessed: 2024-11-29.
- [5] Tom B. Brown, Benjamin Mann, Nick Ryder, et al. Language models are few-shot learners. *arXiv preprint arXiv:2005.14165*, 2020.
- [6] Tom B. Brown, Benjamin Mann, Nick Ryder, Melanie Subbiah, Jared Kaplan, Prafulla Dhariwal, Arvind Neelakantan, Pranav Shyam, Girish Sastry, Amanda Askell, et al. Language models are few-shot learners. *arXiv preprint arXiv:2005.14165*, 2020.
- [7] Lynn Elliot Cannon. *A cellular computer to implement the kalman filter algorithm*. PhD thesis, Montana State University, 1969.
- [8] Cerebras Systems. GEMM with collective operations. Accessed: 2024-10-05.
- [9] Cerebras Systems. Benchmark GEMV collectives, 2023. Accessed: 2024-11-29.
- [10] T. Chen et al. TVM: An automated end-to-end optimization stack for deep learning. *SSP 2018*, 2018.
- [11] Jaeyoung Choi, Jack J. Dongarra, and David W. Walker. Parallel matrix transpose algorithms on distributed memory concurrent computers. *Parallel Computing*, 21(9):1387–1405, 1995.
- [12] Tri Dao. FlashAttention-2: Faster attention with better parallelism and work partitioning. In *The Twelfth International Conference on Learning Representations*, 2024.
- [13] Mark Harris. SambaNova’s new AI chip and the quest for efficiency, 2023. Accessed: 2024-11-29.
- [14] Ke Hong, Guohao Dai, Jiaming Xu, Qiuli Mao, Xiuhong Li, Jun Liu, Kangdi Chen, Hanyu Dong, and Yu Wang. Flashdecoding++: Faster large language model inference on GPUs. *arXiv preprint arXiv:2311.01282*, 2023.
- [15] Norman Jouppi, Cliff Young, et al. Tensor processing units for machine learning: An introduction. Technical report, Google Inc., 2017.
- [16] Jared Kaplan, Sam McCandlish, Tom Henighan, et al. Scaling laws for neural language models. *arXiv preprint arXiv:2001.08361*, 2020.
- [17] Patrick Kennedy. Tenstorrent Blackhole and Metalium for standalone AI processing, 2024. ServeTheHome, Hot Chips 2024 Coverage.
- [18] Jinwoo Kim, Venkata Chaitanya Krishna Chekuri, Nael Mizanur Rahman, Majid Ahadi Dolatsara, Hakki Mert Torun, Madhavan Swaminathan, Saibal Mukhopadhyay, and Sung Kyu Lim. Chiplet/interposer co-design for power delivery network optimization in heterogeneous 2.5-d ICs. *IEEE Transactions on Components, Packaging and Manufacturing Technology*, 11(12):2148–2157, 2021.
- [19] Woosuk Kwon, Zhuohan Li, Siyuan Zhuang, Ying Sheng, Lianmin Zheng, Cody Hao Yu, Joseph Gonzalez, Hao Zhang, and Ion Stoica. Efficient memory management for large language model serving with Page-dAttention. In *Proceedings of the 29th Symposium on Operating Systems Principles*, pages 611–626, 2023.
- [20] Mark LaPedus. TSMC bets big on advanced packaging, 2023. Accessed: 2024-11-29.
- [21] Ching-Jui Lee and Tsung Tai Yeh. ReSA: Reconfigurable systolic array for multiple tiny DNN tensors. *ACM Transactions on Architecture and Code Optimization*, 21(3):43:1–43:24, 2024.
- [22] Zhuohan Li, Lianmin Zheng, Yinmin Zhong, Vincent Liu, Ying Sheng, Xin Jin, Yanping Huang, Zhifeng Chen, Hao Zhang, Joseph E. Gonzalez, and Ion Stoica. AlpaServe: Statistical multiplexing with model parallelism for deep learning serving. In *17th USENIX Symposium on Operating Systems Design and Implementation (OSDI 23)*, pages 663–679, 2023.
- [23] Sean Lie. Cerebras architecture deep dive: First look inside the hardware/software co-design for deep learning. *IEEE Micro*, 43(3):18–30, 2023.
- [24] Yiqi Liu, Yuqi Xue, Yu Cheng, Lingxiao Ma, Ziming Miao, Jilong Xue, and Jian Huang. Scaling deep learning computation over the inter-core connected intelligence processor with T10. In *Proceedings of the ACM SIGOPS 30th Symposium on Operating Systems Principles*, pages 505–521, 2024.
- [25] Liqiang Lu, Naiqing Guan, Yuyue Wang, Liancheng Jia, Zizhang Luo, Jieming Yin, Jason Cong, and Yun Liang. TENET: A framework for modeling tensor

- dataflow based on relation-centric notation. In *2021 ACM/IEEE 48th Annual International Symposium on Computer Architecture (ISCA)*, pages 720–733, 2021.
- [26] Piotr Luczynski, Lukas Gianinazzi, Patrick Iff, Leighton Wilson, Daniele De Sensi, and Torsten Hoefler. Near-optimal wafer-scale reduce. In *Proceedings of the 33rd International Symposium on High-Performance Parallel and Distributed Computing*, HPDC '24, page 334–347. ACM, June 2024.
- [27] Lingxiao Ma, Zhiqiang Xie, Zhi Yang, Jilong Xue, Youshan Miao, Wei Cui, Wenxiang Hu, Fan Yang, Lintao Zhang, and Lidong Zhou. Rammer: Enabling holistic deep learning compiler optimizations with rTasks. In *14th USENIX Symposium on Operating Systems Design and Implementation (OSDI 20)*, pages 881–897, 2020.
- [28] Xiaoning Ma, Qinzhi Xu, Chenghan Wang, He Cao, Jianyun Liu, Daoqing Zhang, and Zhiqiang Li. An electrical-thermal co-simulation model of chiplet heterogeneous integration systems. *IEEE Transactions on Very Large Scale Integration (VLSI) Systems*, 32(10):1769–1781, 2024.
- [29] Meta AI. Introducing MTIA: Meta’s next-generation training and inference accelerator for AI, 2024. Accessed: 2024-12-10.
- [30] Microsoft Azure. Azure Maia: For the era of AI from silicon to software to systems, 2023. Accessed: 2024-11-29.
- [31] Deepak Narayanan, Mohammad Shoeybi, Jared Casper, Patrick LeGresley, Mostofa Patwary, Vijay Korthikanti, Dmitri Vainbrand, Prethvi Kashinkunti, Julie Bernauer, Bryan Catanzaro, Amar Phanishayee, and Matei Zaharia. Efficient large-scale language model training on GPU clusters using Megatron-LM. In *Proceedings of the International Conference for High Performance Computing, Networking, Storage and Analysis*, pages 1–15, 2021.
- [32] NVIDIA Corporation. *cuBLAS: NVIDIA CUDA Basic Linear Algebra Subroutines Library*. NVIDIA, 2023.
- [33] A. Paszke, S. Gross, S. Chintala, et al. Automatic differentiation in PyTorch. *NIPS 2017*, 2017.
- [34] Reiner Pope, Sholto Douglas, Aakanksha Chowdhery, Jacob Devlin, James Bradbury, Jonathan Heek, Kefan Xiao, Shivani Agrawal, and Jeff Dean. Efficiently scaling transformer inference. *Proceedings of Machine Learning and Systems*, 5, 2023.
- [35] J. Rock et al. XLA: Optimizing TensorFlow for high performance. *Google Research*, 2017.
- [36] Yining Shi, Zhi Yang, Jilong Xue, Lingxiao Ma, Yuqing Xia, Ziming Miao, Yuxiao Guo, Fan Yang, and Lidong Zhou. Welder: Scheduling deep learning memory access via tile-graph. In *17th USENIX Symposium on Operating Systems Design and Implementation (OSDI 23)*, pages 701–718, 2023.
- [37] Shukri J. Souri, Kaustav Banerjee, Amit Mehrotra, and Krishna C. Saraswat. Multiple Si layer ICs: motivation, performance analysis, and design implications. In *Proceedings of the 37th Annual Design Automation Conference*, pages 213–220, 2000.
- [38] Emil Talpes, Douglas Williams, and Debjit Das Sarma. DOJO: The microarchitecture of Tesla’s exa-scale computer. In *2022 IEEE Hot Chips 34 Symposium (HCS)*, pages 1–28, 2022.
- [39] R. A. Van De Geijn and J. Watts. SUMMA: scalable universal matrix multiplication algorithm. *Concurrency: Practice and Experience*, 9(4):255–274, 1997.
- [40] Ashish Vaswani, Noam Shazeer, Niki Parmar, Jakob Uszkoreit, Llion Jones, Aidan N. Gomez, Łukasz Kaiser, and Illia Polosukhin. Attention is all you need. In *Advances in Neural Information Processing Systems 30 (NeurIPS 2017)*, pages 5998–6008. Curran Associates, Inc., 2017.
- [41] Lei Wang, Lingxiao Ma, Shijie Cao, Quanlu Zhang, Jilong Xue, Yining Shi, Ningxin Zheng, Ziming Miao, Fan Yang, Ting Cao, et al. Ladder: Enabling efficient low-precision deep learning computing through hardware-aware tensor transformation. In *18th USENIX Symposium on Operating Systems Design and Implementation (OSDI 24)*, pages 307–323, 2024.
- [42] Tianqi Wang, Fan Feng, Shaolin Xiang, Qi Li, and Jing Xia. Application defined on-chip networks for heterogeneous chiplets: An implementation perspective. In *IEEE International Symposium on High-Performance Computer Architecture (HPCA)*, pages 1198–1210, 2022.
- [43] Wikipedia contributors. Static random-access memory, 2024. Accessed: 2024-12-10.
- [44] Wikipedia contributors. Wafer-scale integration, 2024. Accessed: 2024-12-10.
- [45] Bingyang Wu, Shengyu Liu, Yinmin Zhong, Peng Sun, Xuanzhe Liu, and Xin Jin. LoongServe: Efficiently serving long-context large language models with elastic sequence parallelism. In *Proceedings of the ACM SIGOPS 30th Symposium on Operating Systems Principles*, pages 640–654. ACM, 2024.

- [46] Rohan Yadav, Alex Aiken, and Fredrik Kjolstad. DISTAL: the distributed tensor algebra compiler. In *Proceedings of the 43rd ACM SIGPLAN International Conference on Programming Language Design and Implementation*, pages 286–300, 2022.
- [47] Y. Zhao et al. Anso: A compiler stack for auto-tuning tensor programs. *IEEE Transactions on Software Engineering*, 2020.
- [48] Lianmin Zheng, Zhuohan Li, Hao Zhang, Yonghao Zhuang, Zhifeng Chen, Yanping Huang, Yida Wang, Yuanzhong Xu, Danyang Zhuo, Eric P Xing, et al. Alpa: Automating inter-and intra-operator parallelism for distributed deep learning. In *16th USENIX Symposium on Operating Systems Design and Implementation (OSDI 22)*, pages 559–578, 2022.
- [49] Size Zheng, Yun Liang, Shuo Wang, Renze Chen, and Kaiwen Sheng. FlexTensor: An automatic schedule exploration and optimization framework for tensor computation on heterogeneous system. In *Proceedings of the Twenty-Fifth International Conference on Architectural Support for Programming Languages and Operating Systems*, pages 859–873, 2020.
- [50] Yinmin Zhong, Shengyu Liu, Junda Chen, Jianbo Hu, Yibo Zhu, Xuanzhe Liu, Xin Jin, and Hao Zhang. DistServe: Disaggregating prefill and decoding for goodput-optimized large language model serving. In *18th USENIX Symposium on Operating Systems Design and Implementation (OSDI 24)*, pages 193–210. USENIX Association, 2024.
- [51] Yuxiao Zhou and Kecheng Yang. Exploring TensorRT to improve real-time inference for deep learning. In *2022 IEEE 24th International Conference on High Performance Computing & Communications*, pages 2011–2018. IEEE, 2022.
- [52] Hongyu Zhu, Ruofan Wu, Yijia Diao, Shanbin Ke, Haoyu Li, Chen Zhang, Jilong Xue, Lingxiao Ma, Yuqing Xia, Wei Cui, Fan Yang, Mao Yang, Lidong Zhou, Asaf Cidon, and Gennady Pekhimenko. ROLLER: Fast and efficient tensor compilation for deep learning. In *16th USENIX Symposium on Operating Systems Design and Implementation (OSDI 22)*, pages 233–248, 2022.